Meteorol. Atmos. Phys. 41, 165–179 (1989)

Meteorology and Atmospheric Physics

© by Springer-Verlag 1989

551.511.33

DLR Oberpfaffenhofen, Institute of Atmospheric Physics, Federal Republic of Germany

Direct Numerical Simulation of Thermal Convection over a Wavy Surface

K. Krettenauer and **U. Schumann**

With 11 Figures

Received April 14, 1989
Revised May 18, 1989

Summary

The influence of a wavy surface on thermal convection of Rayleigh-Bénard type in a Boussinesq fluid is investigated by direct numerical simulations. The surface height varies sinusoidally in one direction. The wave amplitude amounts up to 10% of the fluid layer height and the wavelength equals about the critical wavelength of Rayleigh-Bénard convection. The horizontal size of the computational domain equals this wavelength. For isothermal no-slip boundaries, two-dimensional convection sets in at subcritical Rayleigh numbers in close agreement with linear theory. The heat-transfer rate grows almost with the square of the surface-wave amplitude. Convection in a fluid layer over a no-slip surface with prescribed heat flux and an adiabatic free-slip boundary at the top is investigated for supercritical Rayleigh numbers and a Prandtl number of 0.7 in two and three dimensions. Two-dimensional simulations show oscillatory roll convection which becomes almost stationary if the Rayleigh number is of order 7000 or less. The two-dimensional convection is unstable with respect to three-dimensional disturbances and a cross-role pattern evolves even over a surface which is undulated in one direction only. For Rayleigh numbers exceeding about 15000, the flow becomes turbulent. The results exhibit little sensitivity of the convection to the wavy surface for a 10% amplitude.

1. Introduction

As a first step towards the understanding of the influence of hilly terrain on convection in the atmospheric boundary layer we investigate in this paper the convection at small and moderate Rayleigh numbers and a Prandtl numbers near unity over a wavy surface with zero mean horizontal motion. Except for the surface wave the problem corresponds to the Rayleigh-Bénard convection case in an infinitely extended Boussinesq fluid-layer with constant material properties heated from below. Thus, we consider a model problem which cannot be compared to real atmospheric conditions directly. However, it should provide some understanding on the potential effect of wavy terrain on atmospheric convection and some guidelines for future case studies. In particular, we will show that the direct forcing of convection by wavy terrain may get reduced by turbulent motions.

With regard to convection over plane surfaces, many studies have considered classical "Rayleigh-Bénard convection (RBC)" as described in Chandrasekhar (1961) for a fluid layer between two no-slip, plane, horizontal, and infinite walls each with uniform but different temperatures. Linear stability analysis shows that convection starts in the form of two-dimensional rolls at a critical (finite) wavelength if the Rayleigh number exceeds a critical value. Chandrasekhar (1961), Sparrow et al. (1963) and Sasaki (1970) have also considered other types of boundary conditions including cases with prescribed heat flux at both boundaries.

However, the case of a fluid layer heated from a no-slip lower surface and topped by an adiabatic free-slip boundary has not yet been considered in the literature. In this case of a "convective boundary layer (CBL)" the heat flux decays linearly from the value at the lower boundary to zero at the top of the layer while the heat flux is constant in the RBC case, and this difference is important with respect to the buoyancy forcing of motions. Therefore, the CBL is more relevant than the RBC to atmospheric conditions. From a linear stability analysis (Krettenauer and Schumann, 1989) we found that the critical Rayleigh number is smaller in the CBL case than in the classical RBC case and convection sets in first at infinitely large wavelength.

Busse (1978) has reviewed the behaviour of nonlinear convection over a plane surface. In the RBC case for increasing Rayleigh number at Prandtl numbers of order unity the roll-convection becomes unstable with respect to three-dimensional disturbances and first an oscillatory type of motion and then non-periodic "turbulent" motions arise for Rayleigh numbers which are about one order of magnitude larger than the critical value (Krishnamurti, 1970). With increasing computer capacities, direct numerical simulations of laminar and turbulent convection became feasible and have been performed by Grötzbach (1982) and (1983). Among others, these studies have confirmed earlier investigations showing an increase of turbulent heat-transfer rate between the two smooth walls in terms of the Nusselt number with the third root of the Rayleigh number. Direct simulations resolve all scales of motion without any subgrid-parametrization but are limited to a finite Rayleigh number of order hundred times the critical value because of limited computer resources. For very large Rayleigh numbers the fully turbulent convection can be investigated by large-eddy simulations as has been done for the atmospheric convective boundary layer over a plane homogeneous surface by Schmidt and Schumann (1989).

Relatively little is known about the impact of heterogeneity of the bounding surfaces. The problem of periodic horizontal disturbances has been investigated analytically for laminar flow by Kelly and Pal (1978) and Pal and Kelly (1978 and 1979). The former showed that the linear analysis of a case with periodic temperature variation at flat walls is closely related to the constant temperature but undulated surface problem. They consider small two-dimensional "resonant" perturbations at a wavelength which equals the critical wavelength of the unperturbated Rayleigh-Bénard problem. The heat-transfer rate increases with the square of the perturbation amplitude. Pal and Kelly (1978) further investigated the problem of non-resonant wavelength exitation due to temperature perturbation. It turned out that sharp bifurcation from conduction to convection at the critical Rayleigh number changes into smooth transition in case of resonant wavelength excitation. Another sharp bifurcation from weak to strong convection occurs for nonresonant excitation as shown by Tavantzis et al. (1978). Pal and Kelly (1979) further considered three-dimensional convection. They found that the two-dimensional flow pattern produced by two-dimensional thermal forcing becomes unstable with respect to three-dimensional disturbances, consisting of two sets of oblique rolls. Hadfield (1988), Schmidt (1988) and Hechtel (1988) have investigated the effects of inhomogeneous surface heating on the turbulent CBL over a flat surface by means of large-eddy simulations. Hadfield (1988) observed a general increase of velocity fluctuations due to an idealized one-dimensional surface heat-flux perturbation. Schmidt (1988) found considerable increase of horizontal velocity fluctuations with increasing inhomogeneity but little effects on the vertical velocity component. Hechtel (1988) simulated an observed case of the CBL with weak mean wind including moisture effects; she found little influence of inhomogeneity on the turbulence statistics.

In this paper, we apply the method of direct numerical simulation to convection over a surface which is sinusoidally undulated in one direction. The wavelength equals approximately the critical wavelength of the plane RBC case. In order to limit the computational effort, the simulation covers just one mode, i.e. the computational domain size corresponds to this wavelength. We consider two types of boundary conditions. The first type corresponds to the classical RBC case with no-slip walls and prescribed uniform temperatures, the lower being warmer than the upper (plane) boundary. The results are compared with the predictions of Kelly and Pal (1978) and this comparison serves to verify the numerical approach

and to confirm older findings on subcritical convection. The method and model parameters are described in chapter 2 and the results are reported in chapter 3. Thereafter, we study boundary conditions which we consider as a fair approximation to the boundary conditions in a CBL as explained above. For this case we do not know of previous investigations to which one could compare the results. In chapter 4, we study the CBL case first two-dimensionally. An interesting question is whether the uni-directional surface height modulation enforces the convection to remain two-dimensional with increasing heat flux. Therefore we consider the same case in three dimensions starting from initial conditions containing small random perturbations. The results for this three-dimensional study are also reported in chapter 4. Chapter 5 summarizes and discusses the results.

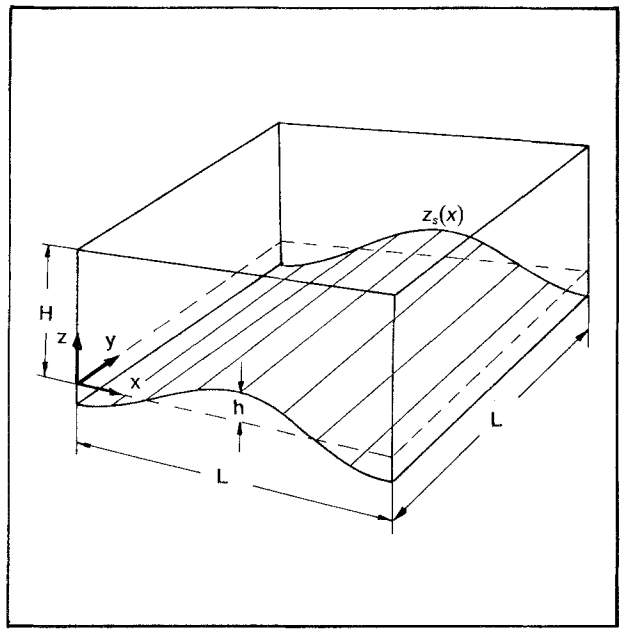

Fig. 1. Perspective sketch of the computational domain in three dimensions showing the sinusoidal surface-wave in x-direction; the surface height is constant in the y-direction

2. Method and Parameters

We consider the flow in a computational domain as shown in Fig. 1. In the two-dimensional case, the flow is invariant with respect to the coordinate y. In the three-dimensional case, the surface height is still invariant in this direction but the flow depends on all coordinates because of small three-dimensional initial disturbances. The flow is bounded from below by a wavy surface with height

$$z_s = h\cos(2\pi x/L)\,, \tag{1}$$

where h and L specify the wave's amplitude and length, respectively. The fluid-layer is topped by a plane horizontal surface at height H. The domain spans horizontally over the length L (in one or two directions) with cyclic boundary conditions. The basic equations describe incompressible flow of a fluid with constant mean density ρ, constant diffusivities ν and μ for momentum and heat, respectively, and constant volumetric expansion coefficient $\beta = -(\partial\rho/\partial T)/\rho$. The Oberbeck-Boussinesq approximation implies constant density except for buoyancy accelerations due to gravity g. We investigate two sets of cases which both include runs with wavy surface but differ in the type of boundary conditions.

The flow is driven in case "RBC" by a prescribed temperature difference ΔT between the upper and lower surface and in case "CBL" by a prescribed kinematic heat flux Q_s from the lower surface while the top surface is adiabatic. The velocity is zero at the lower surface (no-slip). The top surface represents a no-slip boundary in case RBC but a free-slip boundary in case CBL.

In order to reduce the number of independent parameters one introduces nondimensional fields using suitable reference scales. As length scale, the mean height H is selected. With respect to velocity and temperature we have to choose between several alternatives. In the classical RBC, ΔT is the appropriate reference value for temperature. For prescribed heat flux, however, ΔT is an internal parameter and not known a priori. For laminar convection it is common practice to define a temperature scale as a function of the prescribed heat flux, the layer height and the thermal conductivity. However, such a scaling is not suitable for very high Rayleigh numbers where the molecular conductivity becomes unimportant. For the CBL, Deardorff (1970) has identified convective scales which characterize velocity and temperature fluctuations in the fully turbulent situation. We follow this proposal and make all fields non-dimensional by reference to the height H and the velocity and temperature scales which are

$$w_* = (g\beta\Delta TH)^{1/2},\quad T_* = \Delta T\,,\ \text{in case RBC}, \tag{2}$$

$$w_* = (g\beta Q_s H)^{1/3},\quad T_* = Q_s/w_*,\ \text{in case CBL}. \tag{3}$$

In terms of these scales of reference, the non-di-

mensional conservation equations for mass, momentum and internal energy (temperature) are

$$\frac{\partial u_j}{\partial x_j} = 0 \,, \tag{4}$$

$$\frac{\partial u_i}{\partial t} + u_j \frac{\partial u_i}{\partial x_j} = -\frac{\partial p}{\partial x_i} + \frac{1}{Re}\frac{\partial^2 u_i}{\partial x_j^2} + T\delta_{i3} \,, \quad i = 1,2,3, \tag{5}$$

$$\frac{\partial T}{\partial t} + u_j \frac{\partial T}{\partial x_j} = \frac{1}{Re\,Pr}\frac{\partial^2 T}{\partial x_j^2} \,. \tag{6}$$

Here, $u_i = (u, v, w)$, are the Cartesian velocity components, and T, p denote temperature and pressure deviations from an isothermal and hydrostatic reference state, respectively. These non-dimensional fields are functions of the coordinates $x_i = (x, y, z)$ and time t. The coordinate $x_3 = z$ counts vertically upwards and δ_{ij} is the Kronecker delta. As a consequence of the selected reference scales these equations contain the Reynolds and Prandtl numbers

$$Re = \frac{w_* H}{\nu} \,, \quad Pr = \frac{\nu}{\mu} \tag{7}$$

as independent characteristic numbers. Additional numbers characterize the relative amplitude of the wavy surface, $\delta = h/H$, and its wavelength, L/H.

Other reference scales would result in different but related characteristic numbers. Of particular importance is the Rayleigh number

$$Ra = \frac{g\beta T_* H^3}{\nu\mu} = Re^2 Pr \,, \tag{8}$$

which determines the critical conditions for the onset of convection for arbitrary Prandtl numbers in the classical RBC case. For prescribed heat flux as in the CBL case the critical conditions depend on another Rayleigh number

$$Ra_Q = \frac{g\beta Q_s H^4}{\nu\mu^2} = Re^3 Pr^2, \tag{9}$$

again for arbitrary Prandtl numbers (Krettenauer and Schumann, 1989). Thus, for our simulations, Re and Pr are input parameters whereas Ra and Ra_Q will be used as dependent numbers in the discussion.

The initial conditions assume zero velocity; the initial mean temperature decreases linearly with height from the bottom to the top surface in case RBC but is constant in case CBL. Random numbers of order $10^{-3} T_*$ are added to the temperature field to initiate disturbances.

The equations are integrated numerically using the method described in Schumann et al. (1987, the MESOSCOP program, version B). In this method the equations are solved using a coordinate transformation with respect to the vertical coordinate which maps the computational domain on a rectangular one as proposed by Clark (1977). The numerical scheme is based on a staggered grid and finite difference approximations. The momentum and continuity equations are approximated by second-order central differences in space which conserve mass, momentum and energy very accurately. Time integration is performed using the Adams-Bashforth scheme. Advection of temperature is approximated by the second-order upwind-scheme of Smolarkiewicz (1984). This method has been validated by reference to various test cases as described in Schumann et al. (1987).

3. Subcritical Two-Dimensional Rayleigh-Bénard Convection

This chapter reports the results of the simulations of the RBC case which we can compare to the analysis of Kelly and Pal (1978). The selected wavelength of the surface undulation equals the critical wavelength $L = 2.016\,H$ of the classical Rayleigh-Bénard problem for plane surfaces with no-slip conditions on both horizontal walls. The critical Rayleigh number is $Ra = 1\,708$. Here we consider the subcritical range or "quasi-conduction regime" of Rayleigh numbers between 800 and 1 200. The analytical solution for the wavy surface given by Kelly and Pal uses a power series expansion in terms of $\delta = h/H$. For small relative amplitude of the surface elevation ($\delta \leqslant 0.1$), the series contains terms up to second order in δ. The results are found to be independent of the Prandtl number; we choose $Pr = 1$ in the numerical simulations.

For comparison, we evaluate the mean heat-flux across either the lower or upper surface,

$$\bar{Q}_s = \left(\int -(RePr)^{-1}(\partial T/\partial n)\,\mathrm{d}s\right)/\left(\int \mathrm{d}s\right) \,, \tag{10}$$

where n and s denote dimensionless normal and tangential surface coordinates respectively. The upper and lower surface heat fluxes equal each other in the steady state. The ratio of the actual average heat-flux $\bar{Q}_s$ relative to the purely con-

ductive flux in case of zero fluid motion, $\bar{Q}_{cond}$, defines the Nusselt number

$$Nu = \frac{\bar{Q}_s}{\bar{Q}_{cond}} \text{ with } Nu \to 1 \text{ for } Ra \to 0 \,. \tag{11}$$

The purely conductive heat flux $\bar{Q}_{cond}$ is computed by integrating the equations for given geometry with zero buoyancy forces until steady state. Kelly and Pal (1978) found that the increased heat flux due to convective motion scales with the square of the surface-wave amplitude so that $(Nu-1)/\delta^2$ is a pure function of the Rayleigh number.

Subsequently, we compare the numerical results for various values of the Rayleigh number Ra with the corresponding analytical values which are obtained from Fig. 2 b of Kelly and Pal (1978). From Table 1 one can identify the influence of integration time, grid resolution (horizontal times vertical grid-cell numbers), and relative amplitude of the surface variation. For $Ra=800$, the integration results get stationary after $t=6$. At that stage the relative increase of total kinetic energy of fluid motion amounts to about 0.5% per time unit. From theory, $(Nu-1)/\delta^2$ should be independent of δ if δ is taken sufficiently small. In the numerical scheme, we found that too small values of δ below 0.05 induce round-off errors due to small gradients. Therefore, we limited the numerical study to cases with $\delta=0.05$ and 0.1. It is found that a too coarse resolution overestimates the heat transfer. A large value of δ results in a reduced value of this heat transfer. Due to these opposing effects we find that even with poor grid resolution (10×20) the numerical results are in fair agreement with the analytical solution [entry (1) in Table 1]. At doubled grid resolution (20×40) for the same δ, entry (2), the numerical results on $(Nu-1)/\delta^2$ are smaller than the analytical ones. A value of $\delta=0.1$ is about the maximum for which the analytical solution applies. For the same grid resolution and $\delta=0.05$, entry (3), the Nusselt numbers approach the analytical solution again. Results at various integration times, entry (4) and (5) with doubled grid resolution (40×80) show that the discretization effect on the final result is small but the convergence with time towards stationarity declines with increasing Rayleigh number. Such a tendency is to be expected, because the limiting viscous and conductive contributions decay with increasing Rayleigh numbers. Each of these high-resolution calculations took about 1 hour of computer time on a CRAY-XMP. Figure 2 depicts the analytical results together with our "best" numerical data for various values of δ. From this figure, the sensitivity on δ is obvious.

In summary, we find that the computer simulation yields numerical results which are close to the analytical solution of the linear wavy-surface problem. Moreover, we find that the linear solution is limited to small values of δ where the

Table 1. *Results for Two-Dimensional Subcritical Convection*

No.	Discretization	$\delta = h/H$	Total time	Number of time steps	Ra	$(Nu\text{-}1)/\delta^2$ computed	Analyt. value
(1)	10×20	0.1	6.0	1200	800	0.34	0.3
	10×20	0.1	6.0	1200	1000	0.85	0.9
	10×20	0.1	6.0	1200	1200	2.21	2.4
(2)	20×40	0.1	6.0	4800	800	0.30	0.3
	20×40	0.1	12.0	9600	1000	0.73	0.9
	20×40	0.1	12.0	9600	1200	1.86	2.4
(3)	20×40	0.05	6.0	4800	800	0.30	0.3
	20×40	0.05	6.0	4800	1000	0.82	0.9
	20×40	0.05	6.0	4800	1200	2.14	2.4
(4)	40×80	0.05	3.0	9600	800	0.29	0.3
	40×80	0.05	6.0	19200	800	0.30	0.3
	40×80	0.05	12.0	38400	800	0.30	0.3
(5)	40×80	0.05	3.0	9600	1200	1.48	2.4
	40×80	0.05	6.0	19200	1200	2.01	2.4
	40×80	0.05	12.0	38400	1200	2.12	2.4

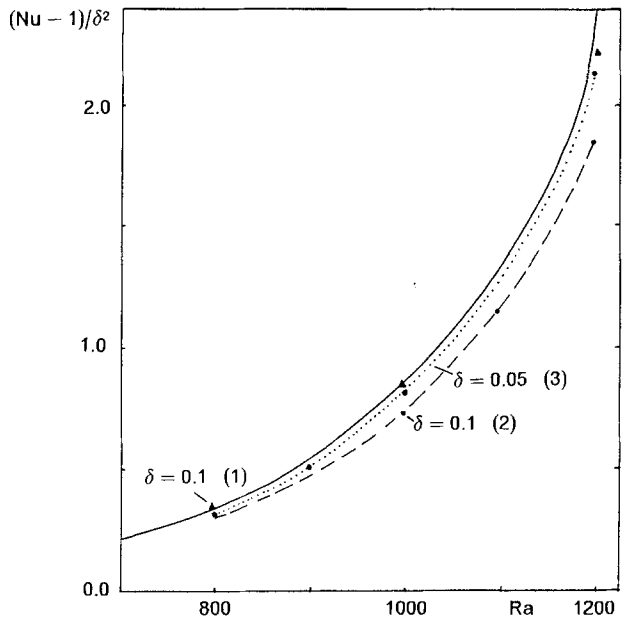

Fig. 2. Rayleigh-number dependence of Nusselt numbers normalized by a function of the surface amplitude $\delta = h/H$, analytical (solid curve) and numerical results (symbols: calculated values, broken lines: estimated values). The numbers in brackets refer to entries in Table 1

actual limit decreases with increasing Rayleigh number but can be estimated to be of order 0.1. For larger values of δ the linear theory overestimates the heat flux.

The results of this chapter can also be regarded as a validation of the computer code. Other reference data are not available to which we could compare the results of the remainder of this paper. However, the test applies for small Rayleigh numbers only where advective fluxes are small. On the other hand, successful tests with dominant advective fluxes have been reported in Schumann et al. (1987).

4. Supercritical Two and Three-Dimensional Convection

In this chapter we investigate the model of a convective boundary layer driven by constant heat flux from a wavy lower surface. Independent parameters are: Re, Pr, L/H, and $\delta = h/H$ for the two-dimensional problems plus the length of the computational domain in the y-direction for the three-dimensional case studies. The rather large computing time for each run with a particular set of parameters, specially for three-dimensional simulations, restricts the range of parameter variations. For the Prandtl number we choose the value $Pr = 0.7$ of air, and fix the lateral domain size and wavelengths at $L/H = 2.0$ (in both directions) for which we expect large effects of the surface undulation. The effect of wavy terrain is identified by comparing cases with $\delta = 0.1$ and $\delta = 0$. Also the numerical resolution is generally kept constant for all the two and three-dimensional cases: $32 \times (16 \times) 40$ grid cells in x, (y,) z-direction, respectively. The finer vertical resolution is taken to resolve the narrow viscous/conductive layer at the lower surface. The coarse grid in y-direction was selected in order to save computer-time because we expected an almost two-dimensional flow pattern. The parameter Re is varied in the range of 100 to 400 and two and three-dimensional cases are considered. Convection sets in for $\delta = 0$ if the Rayleigh number Ra_Q exceeds the value 720 (Krettenauer and Schumann, 1989), which corresponds to the values of $Re_{crit} = 11.4$, and $Ra_{crit} = 90.5$. Thus, we treat supercritical cases and expect to find turbulent flow (in three dimensions). The upper limit of the Reynolds number range considered is about the maximum which can be treated by direct simulations. Grötzbach (1983) discusses the resolution requirements of direct simulations of RBC. He finds that at least three grid points are required within the viscous sublayer for direct numerical simulations. We will show that this requirement is fulfilled in the simulations presented here.

The fluid layer is heated continuously from below and topped by an adiabatic lid. As a consequence the flow approaches a quasi steady-state in which the shape of the horizontal mean temperature profile gets constant after a while whereas the mean temperature increases continously with time. After a transient initial period, the mean motion field becomes stationary when dissipation and buoyancy production of kinetic energy balance each other. For large Reynolds numbers we expect turbulent flow where we can reach stationarity at best in its statistical sense.

It should be pointed out that the lower boundary condition prescribes a heat flux Q_s which is constant and uniform per horizontally projected unit area. As a consequence of this definition the actual surface-specific heat-flux at the inclined surface is less on inclined surface elements that it is on horizontal ones (at most 5% in our case for $\delta = 0.1$ and $L/H = 2$). This method mimics the heat transfer induced by insolation from the nadir.

4.1 General Description of Two and Three-Dimensional Results

In this chapter we describe the results from two and three-dimensional simulations for the fixed Reynolds number of $Re = 150$. Exceptions will be indicated and the effects of higher Reynolds numbers will be reported later.

4.1.1 The Two-Dimensional Case

Figures 3 and 4 show the temperature and velocity-fields as obtained from the two-dimensional simulation at time $t = 30$. At this time, the circulation has reached a quasi-steady state. The flow pattern consists of two counterrotating rolls with their upward branches centred above the surface summit. The heat flux at the inclined surface creates baroclinicity and causes upslope motions symmetrically towards the summit of the surface wave. The fluid near the surface gets heated and reaches maximum temperature at the point of separation from the surface, which coincides with the summit at least initially. The rising fluid reaches maximum vertical velocity little above the middle of the layer. A stagnation point forms above the surface summit at the top boundary where the flow turns aside horizontally. The magnitude of velocity stays approximately constant below the freeslip upper wall because of little internal friction. At the lateral boundaries the flow turns downwards because of the neighbouring cells in the periodic system. Viscous forces in the interior and viscous wall friction at the bottom prevent the flow field from further acceleration. The roll centres are close to points of minimum temperature because they receive heat (at least in steady state) only by lateral diffusion from the main circulation. The equally spaced temperature contours aligned with the surface are consequences of the prescribed conductive heat flux at this boundary. At the top, the contour lines enter perpendicular to the wall because of the adiabatic condition.

Figure 5 shows mean temperature profiles at a sequence of times. These profiles are obtained by averaging along curves $\eta = (\tilde{z} - z_s)/(H - z_s) = \text{const}$ (the tilde denotes the dimensional quantity). Averages along $z = \text{const}$ are not usefull near the lower boundary because the coordinate cuts through the terrain and typical features of the boundary-layer cannot be resolved in that way.

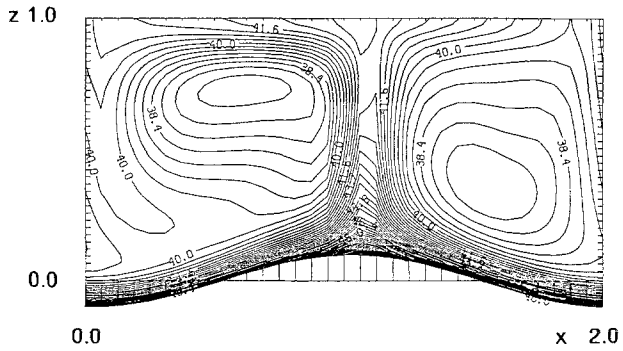

Fig. 3. The temperature field for $Re = 150$, two-dimensional cases at time $t = 30$; the contour-line increment is 0.4

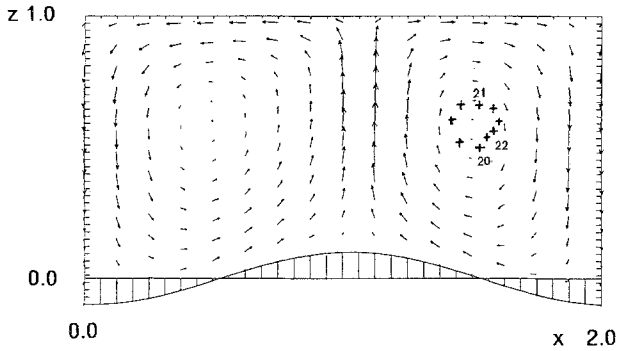

Fig. 4. Velocity field at time $t = 30$ for $Re = 150$; two-dimensional calculation; the maximum vector length is $2.3\, w_*$; the position of the roll centres are marked at times $t = 20.0, 20.25, \ldots, 22$

The profiles show that a quasi-steady shape is achieved after about $t = 10$ with constant increase of mean temperature thereafter. In this limit, the η-averaged vertical heat-flux decreases linearly with height from Q_s at the bottom to zero at the top. Near the surface, the steep normal gradient reflects the purely conductive heat flux Q_s, i.e. $\partial T/\partial n = -Re\,Pr$. The conductive layer extends over about 10% of the entire layer. For a Prandtl number near unity this corresponds to the viscous layer. The depth of this layer should be resolved by at least three grid points to ensure appropriate direct numerical simulation as reported by Grötzbach (1983). Above this viscous layer, the temperature profile is more or less constant with height but the mean temperature rises again in the upper quarter of the fluid layer. Thus heat is transported upwards counter the (positive) gradient of the mean temperature. The physical mechanism of this phenomenon can be clearly understood from the motion pattern shown in Fig. 4. Warm fluid is convected first to the upper boundary and

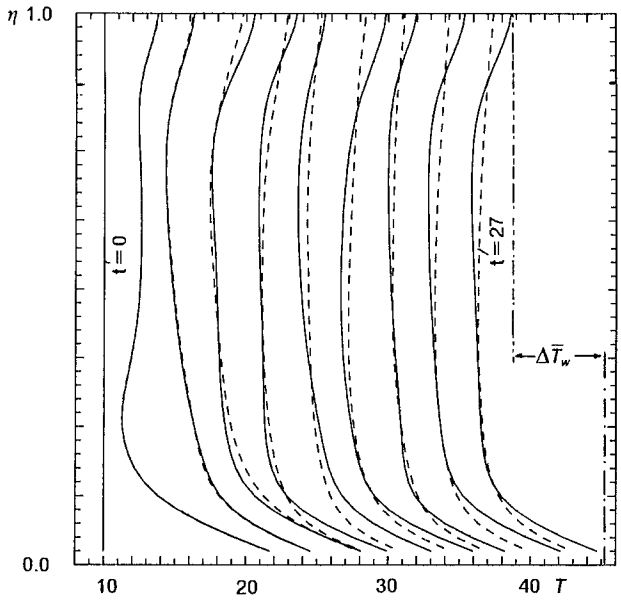

Fig. 5. Mean temperature profiles versus transformed vertical coordinate $\eta=((z\cdot H)-z_s)/(H-z_s)$ for $Re=150$ in the two-dimensional case (solid line) and three-dimensional case (dashed line) at non-dimensional times $t=0$, 3, 6, ..., 27. $\Delta\bar{T}_w$ denotes the mean temperature difference which enters the Nusselt number

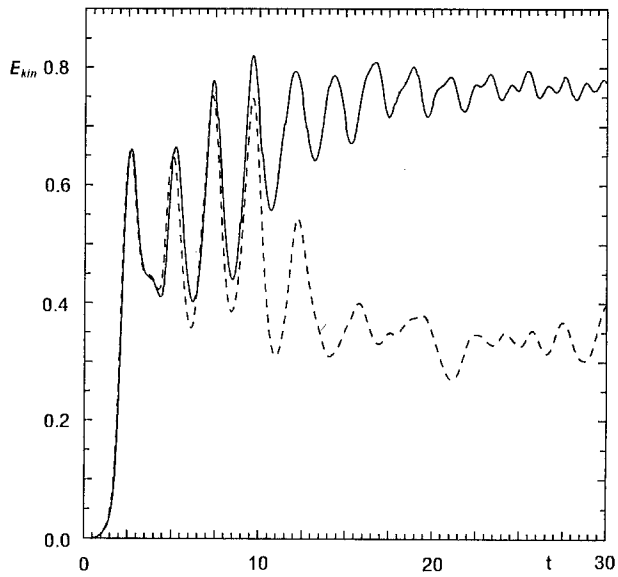

Fig. 6. Mean kinetic energy of the flow field for $Re=150$ as a function of time for the two-dimensional case (solid line) and the three-dimensional case (dashed line)

thereafter contributes to diffusive heating of the fluid inside the rolls. Thus the minimum mean temperature inside the mixed layer is related to the temperature minima in the roll's centres. In contrast to the classical Rayleigh-Bénard convection case, the temperature difference between the two walls is a self adjusting quantity. Its inverse magnitude determines the effective Nusselt number which will be discussed later.

The time dependence of the convection is reflected by Fig. 6 which shows the mean kinetic energy (entire volume average) of the flow field versus time. The graph indicates increase of kinetic energy from zero at the beginning during an acceleration phase until about $t=2.5$. Thereafter, kinetic energy oscillates vigorously with a time period of about 2 time units. This time period is numerically well resolved by about 500 time steps. The oscillations decay slowly with time while the mean level increases monotonically and reaches an asymptotic height.

From an analysis of a time-sequence of plots as shown in Figs. 3 and 4 we found that the energy oscillation is related to a revolution of the roll's centre position along a circle in the rotation sense of the proper roll. The roll's centre at a sequence of non-dimensional times from 20 to 22 is indicated in Fig. 4. This time period corresponds to about one oscillation period. The energy maximum is associated with the upward directed motion of the roll's centre. This oscillation originates from the onset of convection. Initially the motion velocity is small and the fluid layer adjacent to the surface achieves rather high temperature due to the surface heat flux. This fluid layer starts moving upwards departing from the surface's summit and forms two symmetrical small-size eddies initially. When the rather warm fluid volume which originates from the surface layer enters the downward branch it decelerates the whole circulation and accelerates again when entering the upward branch. This results in the main portion of the observed energy oscillation in the initial period. The small-sized initial eddies grow in size and their centres are dragged along with the flow. After some time, the initial disturbances are smoothed out and the rolls finally approach their asymptotic position. A secondary type of oscillation is connected with a small reciprocating motion of the stagnation point at the lid. It occurs only if small random initial disturbances induce asymmetries in the initial conditions. Otherwise, the simulations result in totally symmetric flow patterns but still showing the first type of oscillation.

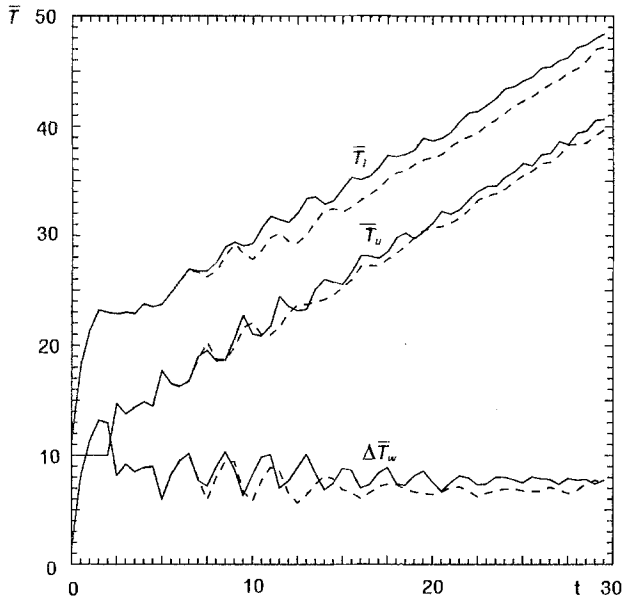

Fig. 7. Mean wall-temperature of the upper ($\bar{T}_u$) and the lower ($\bar{T}_l$) wall and temperature difference $\Delta\bar{T}_w$ versus time for $Re = 150$ (two-dimensional case: solid line; three-dimensional case: dashed line)

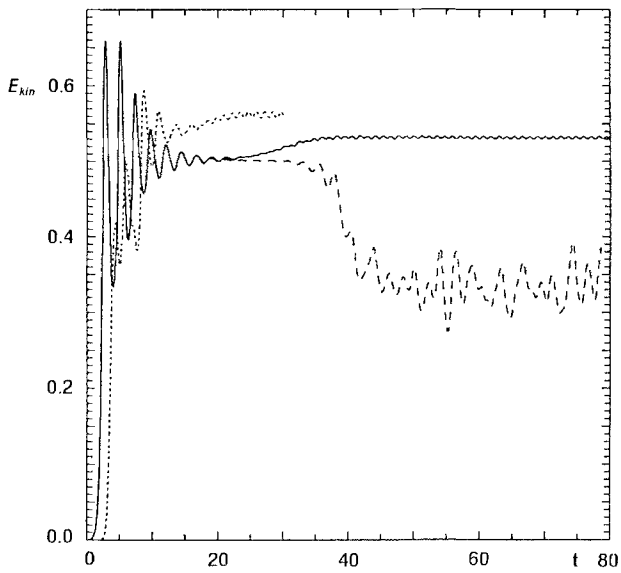

Fig. 8. Mean kinetic energy versus time in the two-dimensional case (solid curve: $\delta = 0.1$, dotted curve: $\delta = 0$, i.e. plane surface) and three-dimensional case (dashed curve: $\delta = 0.1$), for $Re = 100$. Note the sudden decrease of kinetic energy at time $t = 35$ (dashed curve) indicating the transition from two to a three-dimensional convection pattern

The time-dependence of the convection is also reflected by Fig. 7. The mean temperature $\bar{T}_l$ at the lower surface increases first. The mean temperature at the upper surface $\bar{T}_u$ follows when warm fluid reaches the upper boundary. Thereafter, the temperature difference $\Delta\bar{T}_w$ and the mean temperatures at the surfaces reflect the decaying oscillations of the flow pattern. Finally, the temperature difference approaches a constant and the mean temperature increases with unit rate in the present system of reference scales as required by the thermal energy budget.

The effect of the surface wave on the resulting kinetic energy is illustrated in Fig. 8 in which the full curve represents the results of a case with surface undulation for $Re = 100$ while the dotted curve belongs to a plane surface. For a plane surface, the convective motion sets in later and at lower rate because the initial baroclinicity due to the random disturbances is smaller compared to the undulated case. However, the asymptotic value of the kinetic energy in the plane case is less than 10% higher than in the case with a finite surface wave. Also, the flow pattern in the plane case has been found to exhibit the same type of roll-motion as for a wavy surface and the rolls now take fixed but randomly selected lateral positions within the computational domain.

4.1.2 The Three-Dimensional Case

The three-dimensional simulation was carried out with exactly the same parameters as in the two-dimensional case. Only the y-direction was enlarged to the same periodicity-length as the x-direction. Because of the two-dimensional forcing one would expect close similarities between the three and the two-dimensional results. The temperature profiles in Fig. 5 for the three-dimensional case show rather small differences with respect to the two-dimensional results. The region of an almost uniform mean-temperature is now extended to the lid and the thickness of the thermal boundary layer decreased from 10% to about 7% of the height. This is the effect of increased convective mixing in the fluid layer. However, the mean wall-temperature difference remains almost unchanged for small Reynolds numbers (see Fig. 7). Therefore we expect small differences between two and three-dimensional results for the Nusselt numbers. However, there are striking differences concerning the behaviour of the flow field as Fig. 6 exhibits.

The result shown in Fig. 6 indicates that the two cases develop very similarly until non-dimensional time 10. Thereafter the two-dimensional initial flow gets unstable with respect to the small three-dimensional disturbances which had been added initially. The transition from the two to the three-dimensional flow state can occur very suddenly. Figure 8 shows this clearly for the smaller Reynolds number, $Re = 100$. Obviously, the two-dimensional flow tends to reach an asymptotic state when the three-dimensional instability succeeded in changing the flow pattern at time $t = 35$. Test simulations showed no such transition when the random disturbances are set to zero. Moreover, we found that these transitions occur for both free-slip and no-slip top boundary conditions. Thus, the type of top boundary condition is not essential for this instability.

The transition from two to three-dimensional flow is illustrated by Fig. 9 which applies to $Re = 100$ and shows the flow field in the top plane. Initially the two-dimensional rolls form a stagnation line along the y-direction above the summit of the surface wave. An instability seems to start from this stagnation line (the actual y-position must be a consequence of the random initial fields). At later times we see that a secondary roll has been formed with axis perpendicular to the original two-dimensional roll. At $t = 55$, the stagnation line has turned into a stagnation point. The final square pattern shows two rolls of about equal velocity amplitude with little indication of the underlying surface wave. Figure 10 shows contour plots of the vertical velocity on a terrain-following coordinate surface-level $\eta = 0.75$ for selected times and Reynolds numbers. For $Re = 100$ it again clearly reflects the transition from the two-dimensional roll mode to cross-role convection. The results for higher Reynolds numbers will be discussed in the following section.

Figures 6 and 8 show that the mean kinetic energy in the three-dimensional case approaches an asymptotic level which is about half the two-dimensional one. This fact can be explained as follows: The mean buoyancy forcing of energy equals the mean value of wT in non-dimensional units. If the convective heat flux dominates relative to conductive parts, this mean value approaches the same value both in two and three dimensions because of prescribed surface heat flux. The mean buoyancy forcing is actually close to 0.5 because

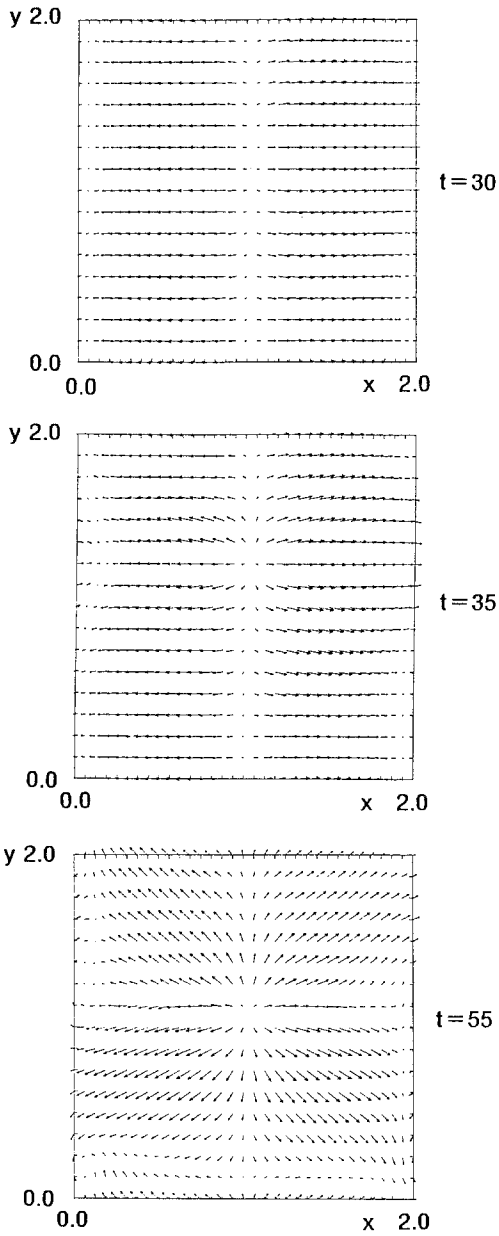

Fig. 9. Velocity-vector plots for $Re = 100$ in horizontal planes near the top surface at three subsequent times. The maximum vector length corresponds to $2.4\, w_*$. The line-convection becomes unstable and the square-pattern convection sets in between $t = 30$ and 35

the heat flux decreases linearly from the surface to the upper boundary. Thus, this forcing is independent of details of the motion field. On the other hand, the amount of viscous dissipation for given energy increases when more than just one basic mode of motion is excited. For the cross-role convection, two modes contribute to dissipation while only one mode dominates in two dimensions. Therefore the energy in this three-

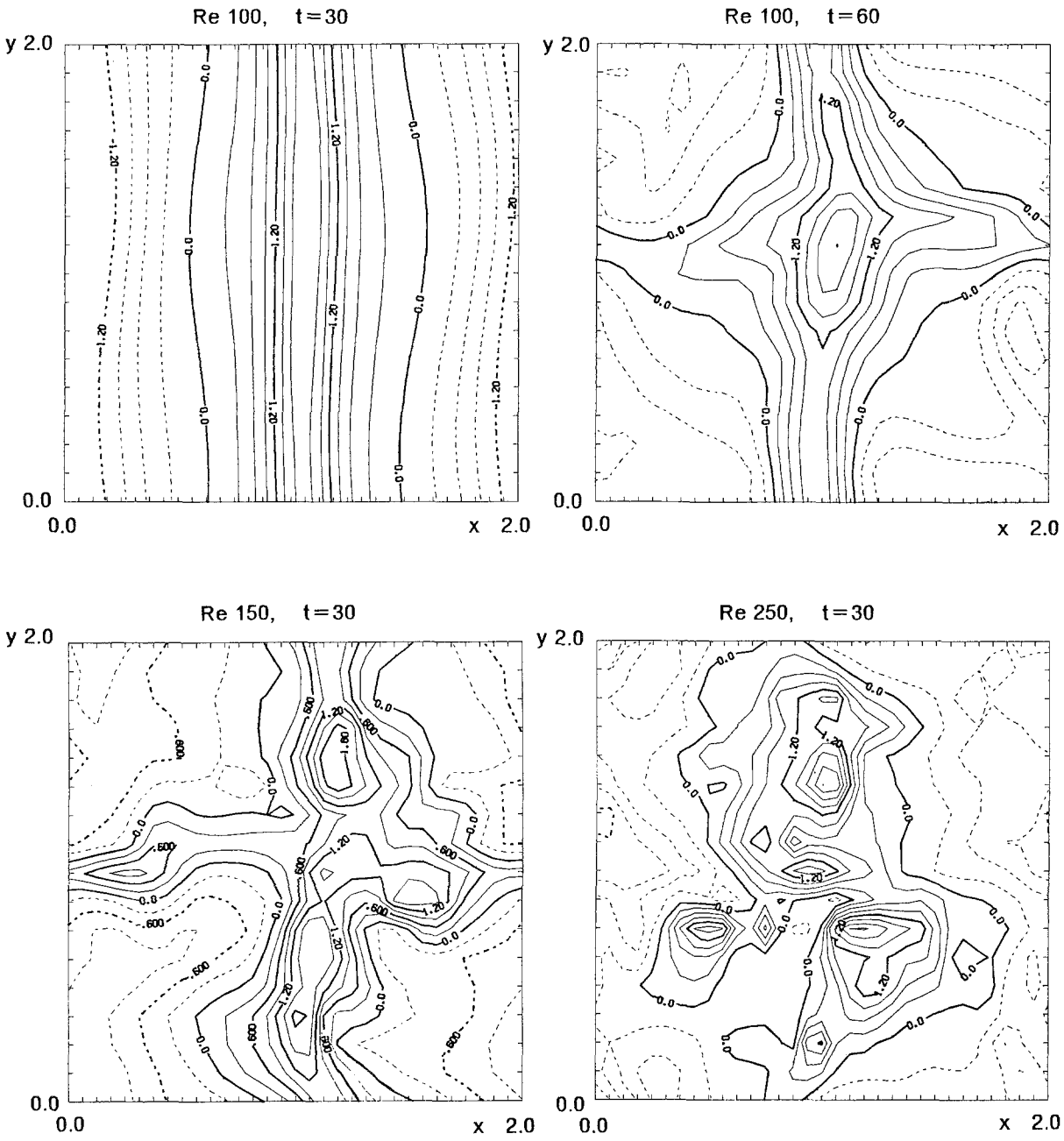

Fig. 10. Contour plots of vertical velocity at $\eta = 0.75$ for different Reynolds numbers and times; contour interval $0.3\, w_*$

dimensional case is about half the value in two dimensions. This ratio will decrease when the flow gets more complicated.

4.2 Effect of Reynolds-Number Variation

4.2.1 The Two-Dimensional Case

In two dimensions, the main effect of increasing the Reynolds number is a reduced damping of the oscillating solutions. The simulations approach a virtually non-oscillating case only for $Re = 100$ where a small (0.5%) remaining amplitude of kinetic energy oscillations is observable in Fig. 8. For higher Reynolds numbers, the flow oscillations grow in amplitude and frequency and the solutions do not seem to approach a steady state in the strict sense.

Results for various Reynolds numbers are summarized in Table 2 for the two-dimensional cases. The given values for maximum velocity, kinetic

energy and temperature difference are averages over the final quasi-steady period of the simulations which is identified with the last 1 000 timesteps of the simulations (about 5 time units).

Table 2 contains also results on the Nusselt number which is defined as before by the ratio of the actual heat flux to that one of the purely conductive situation (with the same mean-temperature difference),

$$Nu = \frac{Q_s}{Q_{cond}} = c\frac{Q_s H}{\mu \Delta \tilde{T}_w} = \frac{c\, Re\, Pr}{\Delta \tilde{T}_w} \tag{12}$$

The tilde denotes dimensional quantities. The coefficient $c = c(\delta)$ accounts for the relationship between the purely conductive heat flux and the mean temperature difference, $Q_{cond} = \mu \Delta \tilde{T}_w/(cH)$. For flat surfaces, its value is $c(0) = 0.5$ as can be seen easily from the analytical asymptotic solution for the conductive case,

$$\tilde{T}(\tilde{z}) = \tilde{T}_0 + \frac{Q_s}{H}\tilde{t} + Q_s \frac{1}{2}\frac{H}{\mu}\left(1 - \frac{\tilde{z}}{H}\right)^2, \tag{13}$$

which yields

$$\Delta \tilde{T}_w = \tilde{T}|_{\tilde{z}=0} - \tilde{T}|_{\tilde{z}=H} = 0.5\, Q_s H/\mu\,. \tag{14}$$

For the undulated surface case, the value of $c(\delta)$ had to be determined numerically by applying the code without gravity forces. This resulted in $c(0.1) = 0.4977$ for the given surface-wave amplitude of $\delta = 0.1$. The inclusion of c in the definition of Nu ensures that $Nu \to 1$ for $Ra \to 0$.

Table 2 contains results from two-dimensional simulations for the standard resolution and results for two runs ($Re = 150$ and 400) with doubled resolution. The differences between the standard grid and the refined grid simulations are small for $Re = 150$. Somewhat larger differences are observed for $Re = 400$ which shows about 20% increase in both kinetic energy and wall temperature-difference compared to the coarse grid-resolution results. These differences are still sufficiently small so that the numerical results can be assumed to be only little influenced by numerical approximation errors.

The mean wall-temperature difference $\Delta \bar{T}_w$ inceases with the Reynolds number but less than linear because of enhanced convective heat transfer. This trend is also reflected in the variation of the Nusselt number as plotted in Fig. 11. The final values of the mean kinetic energy and the maximum vertical velocity of the flow field rises with increasing Reynolds numbers, but slowly.

Table 2 and Fig. 11 contain a few results for a plane lower surface. In this case the Nusselt numbers are smaller but only litte (about 10%). As shown in Fig. 8, the kinetic energy of the plane

Table 2. *Results oof Two-Dimensional Simulations* (bracketed values for fine grid)

Two-dimensional calculations with discretization 40×32 (80×64)						
Reynolds number *Re*	100	150	200	250	300	400
Raleigh number *Ra*	7 000	15 750	28 000	43 750	63 000	112 000
Number of time-steps	12 000 (12 000)	6 000	6 000	9 000	9 450	9 000 (18 000)
Total time (units H/w_*)	15	30	30	28.125	29.53	28.125
CPU-time (min) CRAY-XMP	20	10 (60)	10	15	15	15 (60)
Maximum vertical velocity w_{max}	2.3	2.5 (2.6)	2.7	2.9	3.3	3.3 (3.7)
Kinetic energy	0.53	0.76 (0.79)	0.93	1.07	1.19	1.42 (1.76)
Mean temperature difference $\Delta \bar{T}_w$	6.81 ± 0.37	7.72 ± 0.37 (7.90 ± 0.34)	8.85 ± 0.63	9.70 ± 1.04	10.33 ± 1.42	10.39 ± 2.15 (12.43 ± 1.93)
Nusselt number $Nu = c\, Re\, Pr/\Delta \bar{T}_w$	5.11 ± 0.26	6.77 ± 0.30 (6.56 ± 0.28)	7.87 ± 0.52	8.99 ± 0.83	10.12 ± 1.08	13.41 ± 2.75 (11.20 ± 1.59)
Nusselt number for $\delta = 0$	4.81 ± 0.34		7.30 ± 0.61		9.00 ± 1.03	11.80 ± 2.25

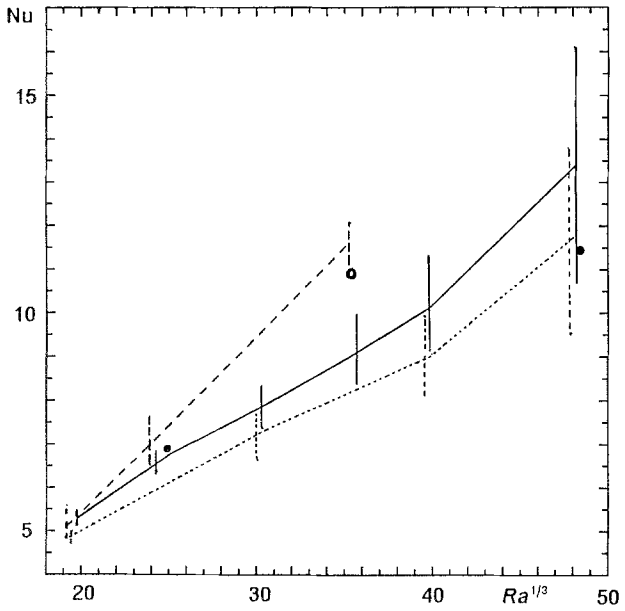

Fig. 11. Nusselt number versus third root of Rayleigh number Ra as obtained from two-dimensional simulations with $\delta = 0.1$ (solid line) and with $\delta = 0$ (dotted line) and from three-dimensional simulations with $\delta = 0.1$ (dashed line). The "error bars" measure the amplitude of the oscillating results in the final period of the simulations. The two single full dots correspond to refined-grid solutions of the two-dimensional case. The single open circle is the result of a three-dimensional simulation for a flat surface ($\delta = 0$)

surface cases is about 10% larger (for $Re = 100$) than for $\delta = 0.1$.

4.2.2 The Three Dimensional Case

Figure 10 shows clearly that a very irregular flow state is approached in three dimensions, at least for $Re \geqslant 150$. This state appears to be non-repeating and thus turbulent.

Table 3 shows various results of the three-dimensional calculations. Only a few cases are considered because such runs are rather expensive in computer time. The Nusselt numbers, see Fig. 11, are somewhat larger than the corresponding two-dimensional values because of an increased heat transfer associated with the turbulent three-dimensional flow. Both the two and the three-dimensional results support a relationship $Nu \sim Ra^{1/3}$. The correspondent graphs of the two-dimensional simulations could be extrapolated linearly to $Ra = 0$ giving approximately the expected value $Nu = 1$. Extrapolation to the laminar Ra-number range is not suitable for the three-dimensional results. The case with plane surface in three dimensions shows even smaller differences to the corresponding undulated surface result than in two dimensions. The maximum vertical velocity and in particular the specific kinetic energy remain considerably smaller than the two-dimensional results, especially at high Reynolds numbers. This is obviously a consequence of the more efficient dissipation in the turbulent three-dimensional flow. The velocity and the kinetic energy values are only very little dependent on the Reynolds number. This shows, that the flow field is suitably scaled in turbulent convection by means of the convective velocity w_* even at these moderate Reynolds numbers.

5. Summary and Conclusions

We have studied subcritical convection between two isothermal no-slip surfaces (RBC) in two dimensions and supercritical convection over a no-slip surface with prescribed heat flux (CBL) in two and three dimensions over wavy and plane surfaces. The surface-height varies sinusoidally in one

Table 3. *Results of Three-Dimensional Simulations*

Three-dimensional calculations with discretization $40 \times 16 \times 32$			
Reynolds number Re	100	150	250
Rayleigh number Ra	7000	15750	43750
Number of timesteps	16000	6000	6000
Total time (unit H/w_*)	80	30	30
CPU-time (hours)	4	2	2
Maximum vertical velocity w_{max}	2.4	2.4	2.3
Kinetic energy	0.34	0.34	0.38
Mean wall-temperature difference $\Delta \bar{T}_w$	6.85 ± 0.79	7.01 ± 0.70	7.50 ± 0.33
Nusselt number $Nu = c\, Re\, Pr/\Delta \bar{T}_w$	5.08 ± 0.49	7.45 ± 0.60	11.61 ± 0.43
Nusselt number for $\delta = 0$			10.88 ± 0.74

direction and the simulation covers only one wave with a wavelength of about twice the layer-height. The main findings of the present study are as follows:

The numerical results for subcritical RBC are in accordance with analytical predictions of Kelly and Pal (1978). Convection sets in over a wavy surface at small Rayleigh numbers and the heat transfer grows with δ^2 as long as $\delta \ll 1$. For finite surface waves, the increase is smaller than suggested by linear theory.

Two-dimensional convection at supercritical Rayleigh numbers in the CBL initiates in an oscillatory manner. Two types of oscillations have been identified, a symmetric one connected with a revolution of the roll centres and an asymmetric one due to sideward oscillation of the upward motion. These oscillations decay and the flow becomes stationary for $Re \leqslant 100$ for the parameters $Pr = 0.7, \delta = 0.1, L/H = 2$ investigated in this study. For larger Reynolds numbers it is not clear whether a steady state is achieved in two dimensions because that requires very long integration times.

The primary rolls are unstable with respect to three-dimensional disturbances even at a Reynolds number $Re = 100$, and a square-roll pattern develops where the rolls in both directions have about equal velocity amplitude. The instability seems to originate from the stagnation line at the top surface. Pal and Kelly (1979) observed a similar instability over a plane surface when the temperature at the lower wall varies periodically in one direction.

For a Reynolds number above about 200, the square-pattern convection develops into an irregular motion pattern which can be classified as being turbulent. This pattern has little resemblence of the underlying two-dimensional surface-wave, at least for $\delta \leqslant 0.1$ and $L/H = 2$.

In the supercritical regime, the effective Nusselt number grows about with the third root of the Rayleigh number. This result is typical for convection over smooth surfaces while other relationships are to be expected for rough surfaces (Schumann, 1988). The three-dimensional motions are more effective in transporting heat than the two-dimensional ones. The effect of the wavy surface on heat transfer is, however, rather small for supercritical convection and the selected surface parameters. This finding is in accordance with results of Hechtel (1988) who found little effect of variable surface heating rates on the CBL over flat terrain. The velocity magnitude is closely related to the convective velocity scale proposed by Deardorff (1970) even for rather moderate Rayleigh numbers, in particular in the three-dimensional (turbulent) flow state.

As a whole, we find strong effects of wavy terrain for small Rayleigh numbers. However, the present study shows that a 10% height variation has little effects on the turbulent convective boundary layer. This seems to be a consequence of the fact that the thermal energy-input is the same over the plane and the undulated surface. The surface heat flux controls the buoyancy forcing. The turbulent convective flow appears to be efficient in converting the buoyancy forcing into kinetic energy even for plane surfaces and the effect of the wavy surface on kinetic energy dissipation is small.

In a future study we plan to examine the influence of other terrain shapes and to extend the simulations to higher Rayleigh numbers by means of large-eddy simulations.

References

Busse, F. H., 1978: Non-linear properties of thermal convection. *Rep. Prog. Phys.*, **41**, 1930–1967.

Chandrasekhar, S., 1961: *Hydrodynamic and Hydromagnetic Stability*. New York: Dover Publications, 643 pp.

Clark, T., 1977: A small-scale dynamical model using a terrain-following coordinate transformation. *J. Comput. Phys.*, **24**, 186–215.

Deardorff, J. W., Convective velocity and temperature scales for the unstable planetary boundary layer and for Rayleigh convection. *J. Atmos. Sci.*, **27**, 1211–1213.

Grötzbach, G., 1982: Direct numerical simulation of laminar and turbulent Bénard convection. *J. Fluid Mech.*, **119**, 27–53.

Grötzbach, G., 1983: Spatial resolution requirements for direct numerical simulation of the Rayleigh-Bénard convection. *J. Comput. Phys.*, **49**, 241–264.

Hadfield, M. G., 1989: The response of the atmospheric convective boundary layer to surface inhomogeneities. Colorado State University, Atmospheric Science Paper No. 433.

Hechtel, L. M., 1988: The effects of nonhomogeneous surface heat and moisture fluxes on the convective boundary layer. Boston: Amer. Met. Soc., 8th Symp. Turbulence and Diffusion, Apr. 25–29, 1988, San Diego, Cal., p. 37–40.

Kelly, R. E., Pal, D., 1978: Thermal convection with spatially periodic boundary conditions: resonant wavelength excitation. *J. Fluid Mech.*, **86**, 433–456.

Krettenauer, K., Schumann, U., 1989: Struktur der konvektiven Grenzschicht bei verschiedenen thermischen Randbedingungen (Structure of the convective boundary layer for various thermal boundary conditions). *Ann. Meteorol.* (N.F.), in press.

Krishnamurti, R., 1970: On the transition to turbulent convection. *J. Fluid Mech.*, **42**, 295–307.

Pal, D., Kelly, R. E., 1978: Thermal convection with spatially periodic nonuniform heatings: nonresonant wavelength excitation. Proc. 6th Int. Heat Transfer Conf. Toronto.

Pal, D., Kelly, R. E., 1979: Three-dimensional thermal convection produced by two-dimensional thermal forcing. Amer. Soc. of Mech. Engineers, paper ASME 79-HT-109, 8 pp.

Sasaki, Y., 1970: Influences of thermal boundary layer on atmospheric cellular conection. *J. Meteor. Soc. Japan*, **48**, 492–501.

Schmidt, H., 1988: Grobstruktur-Simulation konvektiver Grenzschichten (Large-eddy simulation of convective boundary layers). Thesis, University Munich, report DFVLR-FB 88-30, DLR Oberpfaffenhofen, 143 pp.

Schmidt, H., Schumann, U., 1989: Coherent structure of the convective boundary layer deduced from large-eddy simulation. *J. Fluid Mech.*, **200**, 511–562.

Schumann, U., 1988: Minimum friction velocity and heat transfer in the rough surface layer of a convective boundary layer. *Bound-Layer Meteor.*, **44**, 311–326.

Schumann, U., Hauf, T., Höller, H., Schmidt, H., Volkert, H., 1987: A mesoscale model for the simulation of turbulence, clouds and flow over mountains: Formulation and validation examples. *Beitr. Phys. Atmosph.*, **60**, 413–446.

Smolarkiewicz, P. K., 1984: A fully multidimensional positive definite advection transport algorithm with small implicit diffusion. *J. Comput. Phys.*, **54**, 325–362.

Sparrow, E. M., Goldstein, R. J., Jonsson, V. K., 1963: Thermal instability in a horizontal fluid layer: effect of boundary conditions and non-linear temperature profile. *J. Fluid Mech.*, **18**, 513–528.

Tavantzis, J., Reiss, E. L., Matkowsky, B. J., 1978: On the smooth transition to convection. SIAM *J. Appl. Math.*, **34**, 323–337.

Authors' address: Dipl-Ing. Kilian Krettenauer and Prof. Dr. Ulrich Schumann, DLR, Institute of Atmospheric Physics, D-8031 Oberpfaffenhofen, Federal Republic of Germany.

Verleger: Springer-Verlag KG, Mölkerbastei 5, A-1010 Wien. — Herausgeber: Prof. Dr. Elmar R. Reiter, Colorado State University, Ft. Collins, CO 80523, U.S.A. — Redaktion: Türkenschanzstraße 18, A-1180 Wien. — Hersteller: Filmsatz und Offsetdruck: Adolf Holzhausens Nachfolger, Kandlgasse 19-21, A-1070 Wien. — Verlagsort: Wien. — Herstellungsort: Wien. — Printed in Austria.